

# Model Predictive Direct Torque Control: Derivation and Analysis of the Explicit Control Law

Tobias Geyer, *Senior Member, IEEE*

**Abstract**—This paper derives and visualizes the explicit state-feedback control law of model predictive controllers for electrical drives, using model predictive direct torque control (MPDTC) as an illustrative example. The control law is given over the whole state-space and computed in an offline procedure. The availability of the control law allows one to analyze the controller, and to visualize and better understand its behavior and decision making process. Based on this concept, numerous other important tasks can be accomplished, such as stability analysis, feasibility analysis, reduction of the computational effort, derivation of switching heuristics and the further improvement of the closed-loop performance.

**Index Terms**—Model predictive direct torque control, model predictive control, state-feedback control law, variable-speed drives, medium-voltage drives

## I. INTRODUCTION

Model predictive direct torque control (MPDTC) is an emerging control concept for three-phase electrical drive system [1]–[3], adopting the principles of model predictive control (MPC) [4], [5]. MPDTC is particularly well suited for medium-voltage drives, which are based on multi-level voltage source inverters and operate at very low switching frequencies [6]. Compared with state-of-the-art schemes, such as direct torque control (DTC) [7] and field oriented control (FOC) [8] with space vector modulation (SVM), MPDTC achieves a reduction of the switching losses by up to 50% [3] for three-level neutral point clamped inverters. Alternatively, the current or torque distortions can be reduced by the same amount [9]. For five-level topologies, the performance benefits are even more pronounced, as shown in [10] and [11].

Unlike DTC or FOC with SVM, MPDTC is based on an online optimization stage. Given the torque and stator flux references and their estimated values, a suitable inverter switch position is computed, such that the switching effort (either the switching frequency or the switching losses) is minimized. This optimization is based on an internal model of the drive that enables the controller to predict the impact of the switching transitions under consideration. Unlike in DTC, the control law is not directly available—for example in form of a look-up table—and thus cannot be analyzed and visualized, complicating the design process and the understanding of MPDTC.

This issue motivates this paper. The state-feedback control law, which is the control input (the switch position) represented as a function of the state vector over the state-space, is computed, visualized and analyzed. The information and insight thus obtained is not only meant to further the understanding of MPDTC, but is also envisioned to help revise and improve the MPDTC algorithm, e.g. with the aim to lower its computational burden. The techniques proposed in this

paper are directly applicable to other predictive drive control methods, including one-step predictive control [12].

The paper is organized as follows. After describing the drive system case study in the next section, the model predictive control problem is formally stated in Sect. III. The MPDTC solution approach and algorithm is summarized in Sect. IV. The control law for MPDTC is computed, visualized and analyzed in detail in Sects. V and VI. Section VII provides concluding remarks.

## II. DRIVE SYSTEM CASE STUDY

Throughout this paper, we will use normalized quantities. Extending this to the time scale  $t$ , one time unit corresponds to  $1/\omega_b$  seconds, where  $\omega_b$  is the base angular velocity. Additionally, we will use  $\xi(t)$ ,  $t \in \mathbb{R}$ , to denote continuous-time variables, and  $\xi(k)$ ,  $k \in \mathbb{N}$ , to denote discrete-time variables with the sampling interval  $T_s = 25 \mu\text{s}$ .

### A. Reference Frames

All variables  $\xi_{abc} = [\xi_a \ \xi_b \ \xi_c]^T$  in the three-phase system ( $abc$ ) can be transformed to  $\xi_{dq0} = [\xi_d \ \xi_q \ \xi_0]^T$  in the orthogonal rotating  $dq0$  reference frame through  $\xi_{dq0} = \mathbf{P}(\varphi) \xi_{abc}$ , where  $\varphi$  denotes the angle between the  $a$ -axis of the three-phase system and the  $d$ -axis of the reference frame. By aligning the  $d$ -axis with the motor's rotor flux,  $\varphi$  also corresponds to the rotor's angular position, see also Fig. 2. The transformation matrix is given by

$$\mathbf{P}(\varphi) = \frac{2}{3} \begin{bmatrix} \cos(\varphi) & \cos(\varphi - \frac{2\pi}{3}) & \cos(\varphi + \frac{2\pi}{3}) \\ -\sin(\varphi) & -\sin(\varphi - \frac{2\pi}{3}) & -\sin(\varphi + \frac{2\pi}{3}) \\ \frac{1}{2} & \frac{1}{2} & \frac{1}{2} \end{bmatrix}. \quad (1)$$

The reference frame rotates with the angular speed  $\omega_{fr} = \omega_r = d\varphi/dt$ , where  $\omega_r$  is the angular speed of the machine's rotor.

The stationary (i.e. non-rotating)  $\alpha\beta 0$  reference frame is obtained by setting both  $\varphi$  and  $\omega_{fr}$  to zero. The  $d$ - and  $q$ -axes are then referred to as  $\alpha$ - and  $\beta$ -axes, respectively, with the 0-axis remaining unchanged. The transformation from the  $abc$  to the  $\alpha\beta 0$  reference frame is defined as  $\xi_{\alpha\beta 0} = \mathbf{P}(0)\xi_{abc}$ .

### B. NPC Inverter

As an example for a medium-voltage drive system, consider a three-level neutral point clamped (NPC) voltage source inverter with an induction machine, as shown in Fig. 1. The inverter is fed by two constant dc-link voltage sources, and its total dc-link voltage is  $V_{dc} = 5.2 \text{ kV}$ . ABB's 35L4510 4.5 kV 4 kA IGCT and ABB's 10H4520 fast recovery diode are used as semiconductor devices.

Let the integer variables  $u_a, u_b, u_c \in \{-1, 0, 1\}$  denote the switch positions in each phase leg, where the values  $-1, 0, 1$  correspond to the phase voltages  $-\frac{V_{dc}}{2}, 0, \frac{V_{dc}}{2}$ , respectively. The actual voltage applied to the machine terminals is given by

T. Geyer is currently with the Department of Electrical and Computer Engineering, The University of Auckland, New Zealand (e-mail: t.geyer@ieee.org)

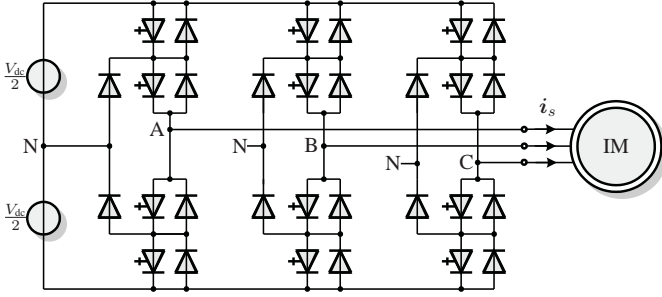


Fig. 1: Three-level neutral point clamped voltage source inverter driving an induction motor with a fixed neutral point potential

$\mathbf{v}_{s,\alpha\beta 0} = 0.5V_{dc} \mathbf{P}(0) \mathbf{u}_{abc}$  with  $\mathbf{u} = \mathbf{u}_{abc} = [u_a \ u_b \ u_c]^T$ . Direct switching between the upper and lower rails is prohibited, i.e.  $\|\Delta \mathbf{u}(k)\|_\infty \leq 1$  is imposed with  $\Delta \mathbf{u}(k) = \mathbf{u}(k) - \mathbf{u}(k-1)$ .

Switching losses arise in the inverter when turning the semiconductors on or off and commutating the phase current. These losses depend on the applied voltage, the commutated current and the semiconductor characteristics. For Integrated Gate Commutated Thyristors (IGCT), with the GCT being the semiconductor switch, the turn-on and turn-off losses can be well approximated to be linear in the dc-link voltage and the phase current. Yet for diodes, the reverse recovery losses are linear in the voltage, but nonlinear in the commutated current.

As shown in [3], [13], the switching losses can be derived as a function of the switching transition, the commutated phase current and its polarity. The turn-on (energy) loss of a GCT, for example, is given by

$$E_{on} = e_{on} \frac{1}{2} V_{dc} i_{ph}, \quad (2)$$

where  $e_{on}$  is a GCT specific coefficient, which is readily available from the manufacturer's data sheets, and  $i_{ph}$  is the phase current. For the GCT turn-off and diode reverse recovery losses, similar equations can be derived.

### C. Induction Machine

The machine considered here is a 3.3 kV and 50 Hz squirrel-cage induction machine rated at 2 MVA. A summary of the machine parameters can be found in Table I. The induction machine is modelled in the  $\alpha\beta$  reference frame using the  $\alpha$ - and  $\beta$ -components of the stator and rotor flux linkages per second,  $\psi_{s\alpha}$ ,  $\psi_{s\beta}$ ,  $\psi_{r\alpha}$  and  $\psi_{r\beta}$ , respectively, as state variables. The rotor speed dynamic is neglected and the rotor's rotational speed  $\omega_r$  is assumed to remain constant within the prediction horizon. The model parameters are the stator and rotor resistances  $R_s$  and  $R_r$ , and the stator, rotor and mutual reactances  $X_{ls}$ ,  $X_{lr}$  and  $X_m$ , respectively. Introducing  $\boldsymbol{\psi}_s = [\psi_{s\alpha} \ \psi_{s\beta}]^T$  and accordingly  $\boldsymbol{\psi}_r$  and  $\mathbf{v}_s$ , the state equations [14] can be written as

$$\frac{d\boldsymbol{\psi}_s}{dt} = -R_s \frac{X_r}{D} \boldsymbol{\psi}_s + R_s \frac{X_m}{D} \boldsymbol{\psi}_r + \mathbf{v}_s \quad (3a)$$

$$\frac{d\boldsymbol{\psi}_r}{dt} = R_r \frac{X_m}{D} \boldsymbol{\psi}_s - R_r \frac{X_s}{D} \boldsymbol{\psi}_r + \omega_r \begin{bmatrix} 0 & -1 \\ 1 & 0 \end{bmatrix} \boldsymbol{\psi}_r \quad (3b)$$

with  $X_s = X_{ls} + X_m$ ,  $X_r = X_{lr} + X_m$  and  $D = X_s X_r - X_m^2$ .

The electromagnetic torque is given by

$$T_e = \frac{X_m}{D} \boldsymbol{\psi}_r \times \boldsymbol{\psi}_s = \sin(\theta) \Psi_s \Psi_r, \quad (4)$$

Induction machine	Voltage	3300 V	$R_s$	0.0108 pu
	Current	356 A	$R_r$	0.0091 pu
	Real power	1.587 MW	$X_{ls}$	0.1493 pu
	Apparent power	2.035 MVA	$X_{lr}$	0.1104 pu
	Frequency	50 Hz	$X_m$	2.3489 pu
	Rotational speed	596 rpm		
Inverter		$V_{dc}$	1.930 pu	

TABLE I: Rated values (left) and parameters (right) of the drive

with the load angle  $\theta$ , which is the angle between the stator and rotor flux vectors. Moreover,  $\Psi_s = \|\boldsymbol{\psi}_s\|$  and  $\Psi_r = \|\boldsymbol{\psi}_r\|$  denote the length of the stator and rotor flux vector, respectively. For more details on the modelling of the induction machine, the reader is referred to [1]–[3] and [14].

## III. MPC PROBLEM FORMULATION

### A. Control Problem

The control problem is to keep the machine's torque and stator flux magnitude within given (hysteresis) bounds around their respective references. During transients, a high dynamic performance is to be ensured, i.e. a short torque settling time in the range of a few ms. Under steady state operating conditions, the total harmonic distortion (THD) of the current is to be kept small, so as to reduce the copper losses and thus the thermal losses in the stator windings of the machine. In addition, to avoid problems with the mechanical load, such as wear of the shaft and the possible excitation of eigenfrequencies of the load, the torque THD needs to be kept at a minimum.

Regarding the inverter, the switching losses in the semiconductors are to be minimized. An indirect way of achieving this is to reduce the device switching frequency.

### B. Target Window

Let  $T_{e,\text{ref}}$  denote the reference of the electromagnetic torque. The upper and lower torque bounds are given by  $T_{e,\text{max}}$  and  $T_{e,\text{min}}$ , respectively. The reference of and bounds on the magnitude of the stator flux vector are defined accordingly as  $\Psi_{s,\text{ref}}$ ,  $\Psi_{s,\text{max}}$  and  $\Psi_{s,\text{min}}$ .

For a given rotor flux vector  $\boldsymbol{\psi}_r$ , the references on the torque and stator flux magnitude can be translated into an equivalent reference stator flux vector  $\boldsymbol{\psi}_{s,\text{ref}}$ , as shown in Fig. 2. The upper and lower torque and flux magnitude bounds can be translated accordingly into the stator flux space, spanned by its  $d$ - and  $q$ -components. These bounds are thus equivalent to a *target window* in the space of the stator flux vector. Keeping the stator flux vector within this window is equivalent to maintaining the electromagnetic torque and the stator flux magnitude within their upper and lower bounds, thus ensuring that the desired electromagnetic torque is generated and that the machine is appropriately magnetized.

Under steady-state operating conditions, the target window rotates in synchronism with the rotor flux vector. Specifically, the target window is stationary within the  $dq$  reference frame, with the torque bounds being parallel to the  $d$ -axis, while the flux bounds are ring segments around the origin. During transients, such as torque steps, the target window is shifted along the  $q$ -axis. In this case, violations of the target window might occur, and the stator flux vector is to be moved back into the target window as quickly as possible, so as to ensure a minimal torque settling time and the avoidance of too high or too low a stator flux magnitude.

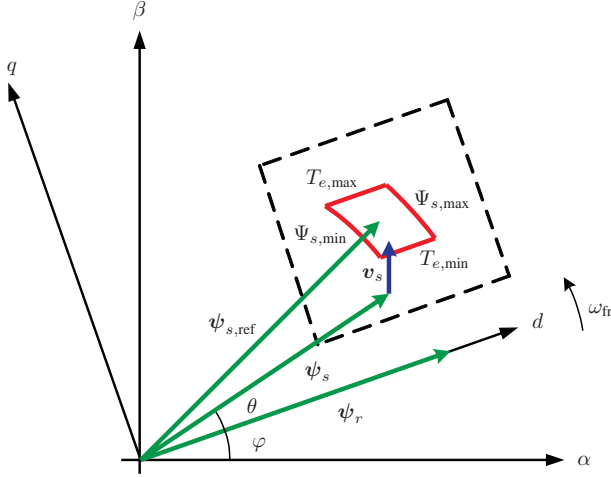


Fig. 2: Stator and rotor flux vectors  $\psi_s$  and  $\psi_r$  in the  $dq$ -reference frame, which rotates with the angular velocity  $\omega_{fr}$ . The target window around the stator flux reference  $\psi_{s,ref}$  is indicated by straight (red) lines, which correspond to the upper and lower bounds on the torque and stator flux magnitude, respectively. The stator flux vector is driven by the voltage vector  $\mathbf{v}_s$ . The dashed (black) lines indicate the rectangular set for which the state-feedback control law will be derived

### C. Optimization Problem

Writing the above control problem as a closed-form optimization problem leads to

$$J^*(\mathbf{x}(k), \mathbf{u}(k-1)) = \min_{\mathbf{U}(k)} (J_{sw} + J_{bnd}) \quad (5a)$$

$$\text{s. t. } \mathbf{x}(\ell+1) = \mathbf{A}\mathbf{x}(\ell) + \mathbf{B}\mathbf{u}(\ell) \quad (5b)$$

$$\mathbf{y}(\ell+1) = \mathbf{g}(\mathbf{x}(\ell+1)) \quad (5c)$$

$$\mathbf{y}(\ell+1) \in \mathcal{Y} \text{ or } \boldsymbol{\varepsilon}_y(\ell+1) < \boldsymbol{\varepsilon}_y(\ell) \quad (5d)$$

$$\mathbf{u}(\ell) \in \mathcal{U}, \quad \|\Delta\mathbf{u}(\ell)\|_\infty \leq 1 \quad (5e)$$

$$\forall \ell = k, \dots, k + N_p - 1, \quad (5f)$$

with  $J^*$  denoting the minimum of the objective function  $J = J_{sw} + J_{bnd}$ . These are a function of the state vector  $\mathbf{x} = [\psi_{s\alpha} \ \psi_{s\beta} \ \psi_{r\alpha} \ \psi_{r\beta}]^T$  at the current time-instant  $k$  and the switch position  $\mathbf{u}(k-1)$ , which was set in the previous control cycle. The sequence of control inputs  $\mathbf{U}(k) = [\mathbf{u}(k), \dots, \mathbf{u}(k+N_p-1)]$  over the prediction horizon  $N_p$  represents the sequence of inverter switch positions the controller decides upon. The objective function (5a) is minimized for all  $\mathbf{U}(k)$  subject to the dynamical evolution of the machine (5b), its outputs (5c) and the constraints (5d) and (5e).

### D. Objective Function

The objective function consists of two parts: The first part  $J_{sw}$  captures the switching effort. Specifically,

$$J_f = \frac{1}{N_p} \sum_{\ell=k}^{k+N_p-1} \|\Delta\mathbf{u}(\ell)\|_1 \quad (6)$$

represents the sum of the switching transitions (number of commutations) over the prediction horizon divided by the length of the horizon—it thus approximates the short-term switching frequency. Alternatively, the switching (power) losses can be directly represented through

$$J_P = \frac{1}{N_p} \sum_{\ell=k}^{k+N_p-1} E_{sw}(\mathbf{x}(\ell), \mathbf{u}(\ell), \mathbf{u}(\ell-1)), \quad (7)$$

which is the sum of the instantaneous switching (energy) losses  $E_{sw}$  over the prediction horizon. Note that, according to (2),  $E_{sw}$  is a function of the stator current  $\mathbf{i}_s$ , which in turn linearly depends on the state vector  $\mathbf{x}$ . In (5a) we either use  $J_{sw} = J_f$  or  $J_{sw} = J_P$ .

The drive's output vector  $\mathbf{y} = [T_e \ \Psi_s]^T$  represents the electromagnetic torque and the stator flux magnitude. To quantify the degree of a bound violation, we introduce for the torque

$$\varepsilon_T = \begin{cases} T_e - T_{e,max} & \text{if } T_e \geq T_{e,max} \\ T_{e,min} - T_e & \text{if } T_e \leq T_{e,min} \\ 0 & \text{else} \end{cases} \quad (8)$$

and accordingly  $\varepsilon_\Psi$  for the stator flux magnitude. The violation of the output vector is then  $\boldsymbol{\varepsilon}_y = [\varepsilon_T \ \varepsilon_\Psi]^T$ .

The second term in the objective function (5a) penalizes the output vector  $\mathbf{y}$  violating its bounds. This term is defined as

$$J_{bnd} = q \boldsymbol{\varepsilon}_y^T \boldsymbol{\varepsilon}_y, \quad (9)$$

with  $q$  being a scalar weighting term and  $\boldsymbol{\varepsilon}_y$  denoting the rms output violation within the prediction horizon of length  $N_p$ . The first component of  $\boldsymbol{\varepsilon}_y$  is given by

$$\varepsilon_T(k) = \sqrt{\frac{1}{N_p} \sum_{\ell=k}^{k+N_p-1} (\varepsilon_T(\ell))^2}, \quad (10)$$

and the second component is defined accordingly.

### E. Internal Prediction Model

The internal prediction model is derived by rewriting the continuous-time machine equations (3) in the state-space form  $\frac{d\mathbf{x}}{dt}(t) = \mathbf{F}\mathbf{x}(t) + \mathbf{G}\mathbf{u}(t)$ . The exact Euler discretization method is used to derive the discrete-time matrices

$$\mathbf{A} = e^{\mathbf{F}T_s} \text{ and } \mathbf{B} = -\mathbf{F}^{-1}(\mathbf{I} - \mathbf{A})\mathbf{G} \quad (11)$$

for the discrete-time state-space representation of the machine model (5b), with  $e$  denoting the matrix exponential,  $T_s$  the sampling interval and  $\mathbf{I}$  the identity matrix. As mentioned earlier, the motor speed is assumed to be constant within the prediction horizon—the speed is thus not part of the state vector but rather a parameter of the model (5b).

### F. Constraints

The upper and lower bounds form the set  $\mathcal{Y} = [T_{e,min}, T_{e,max}] \times [\Psi_{s,min}, \Psi_{s,max}]$ . The constraint (5d) is imposed componentwise, i.e. separately for the torque and the stator flux magnitude. If an output component is at time-step  $k$  within its bounds, then it has to stay within them. This is the standard case during steady-state operation. If, however, a component at time-step  $k$  violates its bound, then it has to move closer to the bounds at every time-step  $\ell$  within the prediction horizon, whereas  $\ell = k, \dots, k + N_p - 1$ .

The constraint (5e) limits the control input  $\mathbf{u}$  to the integer values  $\mathcal{U} = \{-1, 0, 1\}^3$  available for the three-level inverter. Switching in a phase by more than one step up or down is not allowed. This is enforced by the second constraint in (5e),  $\|\Delta\mathbf{u}(\ell)\|_\infty \leq 1$ , which limits the elements in  $\Delta\mathbf{u}$  to  $\pm 1$ . These constraints have to be met at every time-step  $\ell$  within the prediction horizon.

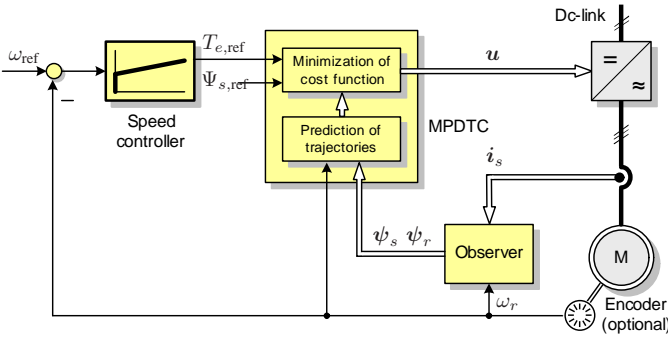


Fig. 3: Model predictive direct torque control (MPDTC) for a voltage source inverter driving an electrical machine

## IV. MODEL PREDICTIVE DIRECT TORQUE CONTROL

### A. MPDTC Solution Approach

The above optimization problem can be solved in real-time by a tailored approach that relies on the fact that switching is mainly required in the vicinity of the bounds or when bounds have been violated. When the torque and stator flux magnitude are well within their bounds, switching is not required and the switch position is frozen.

This gives rise to two different prediction horizons—the switching horizon (the number of switching instants within the horizon, i.e. the controller’s degrees of freedom) and the prediction horizon (the number of time-steps MPDTC looks into the future). Between the switching instants the switch positions are frozen and the drive behavior is extrapolated until a hysteresis bound is hit. The concept of extrapolation leads to long prediction horizons (typically 10 to 100 time-steps), while the switching horizon is very short (usually one to three). The switching horizon is composed of the elements ‘S’ and ‘E’, which stand for ‘switch’ and ‘extrapolate’ (or more generally ‘extend’), respectively. We use the task ‘e’ to add an optional extension leg to the switching horizon. For more details about the concept of the switching horizon, refer to [3].

### B. MPDTC Algorithm

The drive’s system state is fully described by the pair  $\mathbf{x}(k)$  and  $\mathbf{u}(k-1)$ , i.e. the machine state and the previously chosen inverter switch position. Based on those, the optimal control input  $\mathbf{u}^*(k)$  can be computed according to the following procedure.

- 1) Initialize the root node with the current state vector  $\mathbf{x}(k)$ , the switch position  $\mathbf{u}(k-1)$  and the switching horizon. Push the root node onto the stack.
- 2a) Take the top node with a non-empty switching horizon from the stack.
- 2b) Read out the first element. For ‘S’, branch on all feasible switching transitions, according to (5e). Use the internal prediction model (5b) to compute the state vector at the next time-step. For ‘E’, extend the trajectories either by using extrapolation, as detailed in [1], [2], or by using extrapolation with interpolation, as proposed in [15].
- 2c) Keep only the switching sequences that meet (5d).
- 2d) Push these sequences onto the stack.
- 2e) Stop if there are no more nodes with non-empty switching horizons. The result of this are the switching sequences  $\mathbf{U}^i(k) = [\mathbf{u}^i(k), \dots, \mathbf{u}^i(k + N_p^i - 1)]$  over the

variable-length prediction horizons  $N_p^i$ , where  $i \in \mathcal{I}$  and  $\mathcal{I}$  is an index set.

- 3) Compute for each sequence  $i \in \mathcal{I}$  the associated cost  $J_i$ , as defined in (5a).
- 4) Choose the switching sequence  $\mathbf{U}^* = \mathbf{U}^i(k)$  with the minimal cost, where  $i = \arg \min_{i \in \mathcal{I}} J_i$ .
- 5) Apply (only) the first switch position  $\mathbf{u}^*(k)$  out of this sequence and execute the above procedure again at the next time-step  $k+1$ .

For an in-depth description and analysis of this algorithm, the reader is referred to [2], [3]. It is straightforward to consider the balancing of a neutral point potential, see e.g. [2], [3]. Branch and bound techniques can be used to reduce the computation time [16] by an order of magnitude. As shown in Fig. 3, MPDTC constitutes an inner torque and flux control loop, which is typically augmented by an outer speed control loop. Depending on the operating point (speed and torque) the torque and stator flux bounds are adjusted by an external loop so as to maintain an acceptable switching frequency.

## V. CONTROL LAW FOR A GIVEN ROTOR FLUX VECTOR

The control law is the control input represented as a function of the state vector over the state-space  $\mathcal{X}$  of interest, i.e.

$$\mathbf{u}^*(k) = \mathbf{f}_{\text{MPC}}(\mathbf{x}(k)) \quad \forall \mathbf{x} \in \mathcal{X}. \quad (12)$$

### A. Assumptions and Settings

In general, not the whole four-dimensional state-space is of interest. Assume that the machine operates with a constant rotor flux magnitude. This reduces the dimension of the state-space from four to three, with the remaining state variables being the stator flux vector in  $d$  and  $q$ , and the angular position of the rotor flux vector  $\varphi$ . We also assume, without loss of generality, that the machine operates at a constant speed. This implies that the  $dq$  frame rotates with a constant angular velocity.

In the sequel, if not otherwise stated, the operating point is at nominal speed and torque, i.e.  $w_e = 1$  pu and  $T_{e,\text{ref}} = 1$  pu. The magnitude of the rotor flux vector is  $\|\psi_r\| = 0.92$ , ensuring that the rotor dynamics are at steady-state. This implies that the stator flux reference vector in  $dq$  is  $\psi_{s,\text{ref}} = [0.972 \ 0.235]^T$ . The bounds on the electromagnetic torque are chosen as  $T_{e,\text{min}} = 0.85$  and  $T_{e,\text{max}} = 1.15$ , whereas the bounds on the stator flux magnitude are  $\Psi_{s,\text{min}} = 0.97$  and  $\Psi_{s,\text{max}} = 1.03$ . This defines the target window around  $\psi_{s,\text{ref}}$ .

Consider the switching horizon ‘SE’<sup>1</sup> and the objective function  $J = J_P + J_{\text{bnd}}$  in (7), which targets the switching losses. The penalty on the bound violation is set to  $q = 2$ . The control law is derived for stator flux vectors within the dashed rectangle in Fig. 2 and for the rotor flux angle  $\varphi(k) = 0$ . The dashed rectangle is centered around the stator flux reference vector, its edges are parallel to the  $d$ - and  $q$ -axis, and the length of its edges is chosen to be 0.16 pu. Along with  $\|\psi_r\|$  defined above, this determines the subset  $\mathcal{X}$  of the state-space, in which the control law is to be computed.

<sup>1</sup>Recall that ‘SE’ implies that switching is considered only at time-step  $k$ . From time-step  $k+1$  onwards, the switch position is frozen and the output trajectories are extended or extrapolated until a bound is hit.

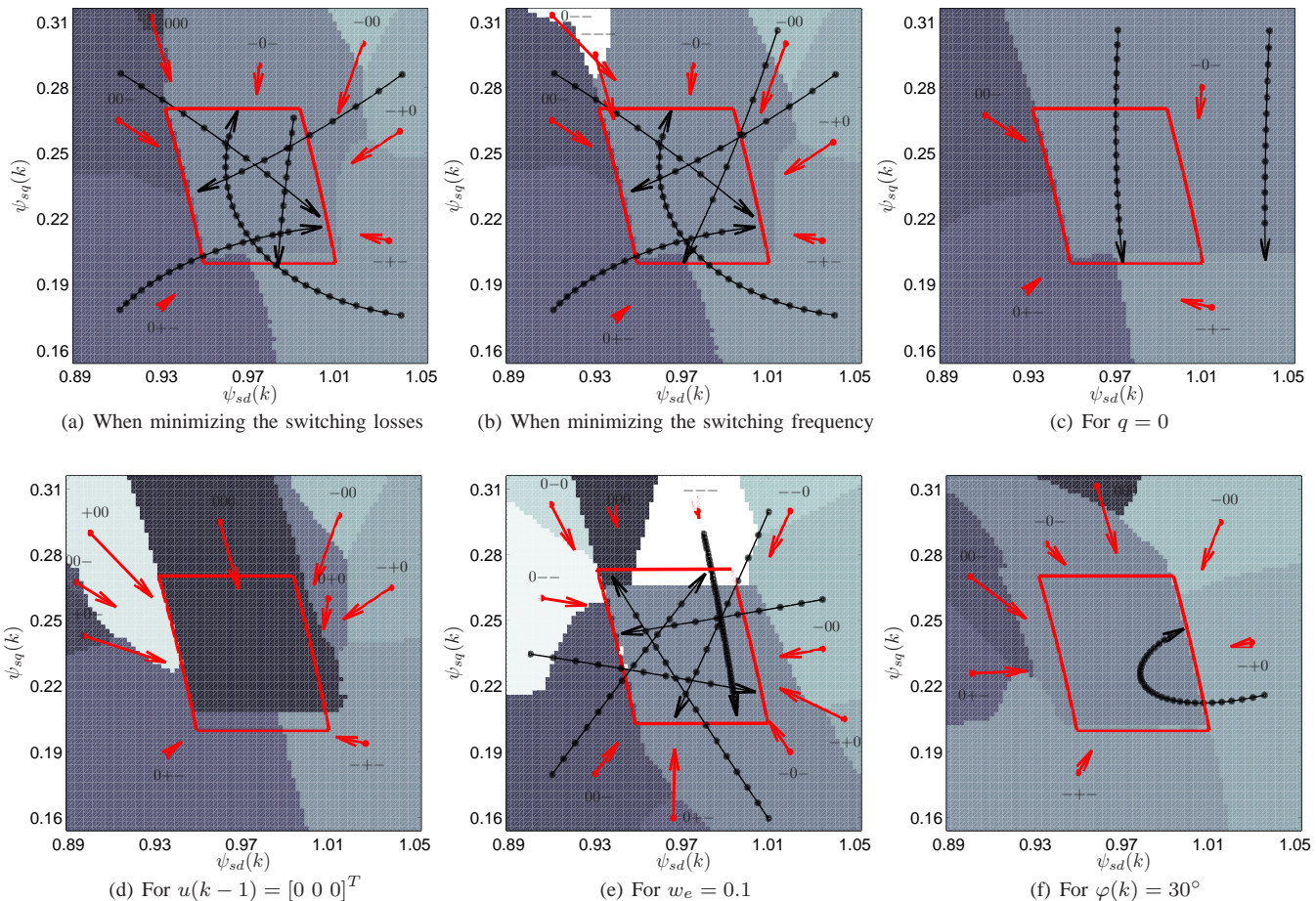


Fig. 4: State-feedback control laws, i.e. inverter switch positions  $\mathbf{u}^*(k)$  as a function of the state vector  $\mathbf{x}(k)$ , for the inverter switch position  $\mathbf{u}(k-1)$  and the rotor flux angle  $\varphi(k)$ . Predicted stator flux trajectories are shown as black lines, while the target window is indicated by straight (red) lines. The (red) arrows indicate the voltage vectors

### B. Algorithm

In order to compute the control law the stator flux vector is varied within the dashed rectangle. Specifically, a fine grid is generated along the  $d$ - and  $q$ -axis that corresponds to stator flux positions within the rectangle. These grid points, along with  $\varphi$  and  $\|\psi_r\|$  fully define the machine's state vector  $\mathbf{x}$ . Then, for a given switch position  $\mathbf{u}(k-1)$ , the control input can be computed for each grid point, yielding the state-feedback control law. The latter can be stored in a table.

### C. State-Feedback Control Law

Several control laws, which resulted from this procedure, are shown in Fig. 4. The control laws  $\mathbf{u}^*(k)$ , i.e. the optimal switch positions, are plotted in the two-dimensional state-space, which is defined by  $\psi_s$ . Different shades of grey are used to indicate the control laws. As can be seen, neighboring state vectors (grid points) refer to the same control law, forming distinctive regions in the state-space, which share the same control law. The control laws of these regions are indicated using the notation  $+$ ,  $0$  and  $-$ . For example,  $00-$  refers to  $\mathbf{u}^*(k) = [0 \ 0 \ -1]^T$ .

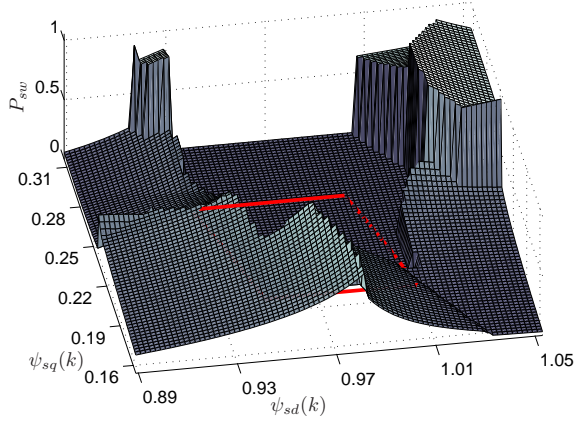
The target window is shown as the slightly curved parallelogram with straight (red) lines. The (red) arrows correspond to the voltage vectors in  $dq$ . The length of the arrows indicates the distanced by which the stator flux vector is moved within

$100 \mu\text{s}$ . These voltage vectors highlight the different velocities by which and the directions in which the different switch combinations drive the stator flux vector relative to the rotating  $dq$  reference frame.

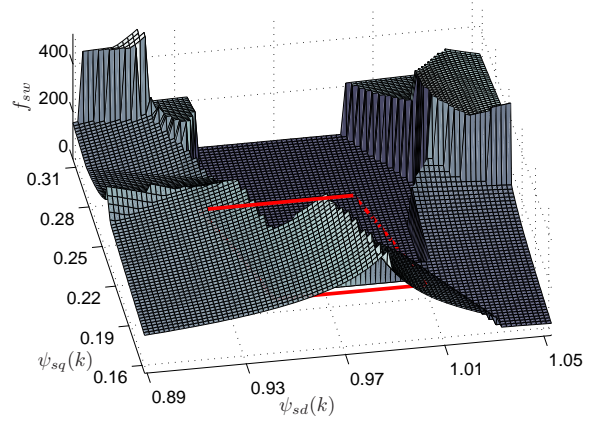
Moreover, predicted stator flux trajectories that correspond to the respective control input, are shown for several regions. Every second sampling instant (i.e. every  $50 \mu\text{s}$ ) along the trajectories is indicated by a small circle. These trajectories start at selected stator flux vectors and terminate when a bound is about to get violated, thus predicting that switching will be required at this point in the future. The length of the trajectories corresponds to the prediction horizon  $N_p$ . For the stator flux trajectory starting in the lower right region with  $\mathbf{u}^*(k) = [-1 \ 1 \ -1]^T$ , for example, the prediction horizon is  $N_p = 53$  steps or  $1.325 \text{ ms}$ . Also note that in the  $dq$  reference frame, in general, voltage vectors move the stator flux along curved rather than straight lines.

### D. Analysis and Observations

In the following details about the individual control laws in Fig. 4 are provided. The control law in Fig. 4(a) is based on the assumptions and settings stated in Sect. V-A. The switching losses are minimized. The current switch position is  $\mathbf{u}(k-1) = [-1 \ 0 \ -1]^T$ , while in Fig. 4(d) it is the zero vector  $\mathbf{u}(k-1) = [0 \ 0 \ 0]^T$ .



(a) Device switching losses  $P_{sw}$  in kW when minimizing the switching losses



(b) Device switching frequency  $f_{sw}$  in Hz when minimizing the switching frequency

Fig. 5: Predicted switching effort, discounted over the prediction horizon, as a function of the state vector  $\mathbf{x}(k)$  for the current inverter switch position  $\mathbf{u}(k-1) = [-1 \ 0 \ -1]^T$ . The target window is indicated by straight (red) lines

The resulting regions have clearly defined borders, forming distinctive areas in the state-space in which the same control input (switch position) is used. When the stator flux vector at time-step  $k$  is within the target window, as exemplified by the almost vertical trajectory in Fig. 4(a), switching is not required and thus avoided (this will be explained in more detail in Sect. V-E). As a result, within the target window, the control law heavily depends on  $\mathbf{u}(k-1)$ , since this largely determines the switching losses and thus the overall cost.

The controller predicts when the target window will be violated and aims to switch such that any violation is avoided. As an example for this, consider in Fig. 4(a) the lower edge of the target window, which refers to the lower torque bound. Here, switching is performed already when the stator flux is one sampling interval away from the lower torque bound. This time-interval translates to different distances in the state-space, depending on the velocity of the voltage vector relative to the  $dq$  frame. This can be observed when comparing Figs. 4(a) and 4(d).

When the stator flux vector is significantly outside of the target window, however, the control laws<sup>2</sup> tend to become similar, irrespective of  $\mathbf{u}(k-1)$ . This can be seen when comparing Figs. 4(a) and 4(d), which only differ with respect to  $\mathbf{u}(k-1)$ . The reason for this is that well outside of the bounds, in the objective function, the bound violation term  $J_{bnd}$ , which is independent of  $\mathbf{u}(k-1)$ , dominates over the switching effort term  $J_{sw}$ . Moreover, the second part of the constraint (5d) ensures that only voltage vectors are considered that move the stator flux vector closer to the target window.

When the switching frequency (rather than the switching losses) is minimized, only small modifications in the resulting control law result, as shown in Fig. 4(b). Differences arise mostly with regards to the common mode of the voltage vectors, as can be seen in the upper left corner of the figure. When switching from  $\mathbf{u}(k-1) = [-1 \ 0 \ -1]^T$  to a zero vector is required, two options exist, namely  $\mathbf{u}(k) = [-1 \ -1 \ -1]^T$

<sup>2</sup>To be precise, the differential mode of the voltage vectors becomes similar. As an example for this, consider in Fig. 4(d) the region with  $\mathbf{u}^*(k) = [0 \ 1 \ 0]^T$  that corresponds in Fig. 4(a) to the region with  $\mathbf{u}^*(k) = [-1 \ 0 \ -1]^T$ .

and  $\mathbf{u}(k) = [0 \ 0 \ 0]^T$ . The first option involves only one switching transition, which is preferable when minimizing the switching frequency. The second option involves two switching transitions, but since the related phase currents are very small in this case, it is advantageous to switch twice, when minimizing the switching losses.

These differences are also reflected in Fig. 5, which shows the predicted switching efforts for the two control laws discussed above. The predicted switching losses in kW are obtained by dividing  $J_P$  by  $1000 T_s$ . A subsequent division by 12 yields the average switching losses per semiconductor device, which are depicted in Fig. 5(a). The switching frequency is obtained accordingly.

Within the regions, as can be seen, the surfaces of the switching efforts are smooth. When moving from one region to a neighboring one, the transition is smooth, if both control laws meet the constraint (5d) at the intersection. As an example, consider the regions with the control inputs  $\mathbf{u}^*(k) = [0 \ 1 \ -1]^T$  and  $\mathbf{u}^*(k) = [-1 \ 1 \ -1]^T$ . If, however, one of the control inputs ceases to meet the constraint (5d), then the switching effort at the transition changes in a step-wise fashion, when moving from one region to a neighboring one. This can be seen at the boundary between the regions with  $\mathbf{u}^*(k) = [-1 \ 0 \ -1]^T$  and  $\mathbf{u}^*(k) = [0 \ 1 \ -1]^T$ . When moving from the first region towards the second one, the control input ceases to meet the constraint, triggering a switching transition and a step-wise change in the switching effort.

Next, consider the control law depicted in Fig. 4(c), which is obtained by setting  $q$  to zero. As a result, only the switching losses are penalized, but no incentive is provided to move the stator flux vector quickly back into the target window. The region in which the former control input is kept, i.e.  $\mathbf{u}^*(k) = \mathbf{u}(k-1)$ , is now much enlarged. In this region, as exemplified for the two predicted stator flux trajectories shown in Fig. 4(c), the degree of the bound violation decreases at every time-step. The second constraint in (5d) is thus met, but the convergence rate is low for the rightmost trajectory. Note that this trajectory terminates when the lower torque bound and hence the constraint (5d) is about to be violated.

Fig. 4(e) shows the control law when lowering the speed

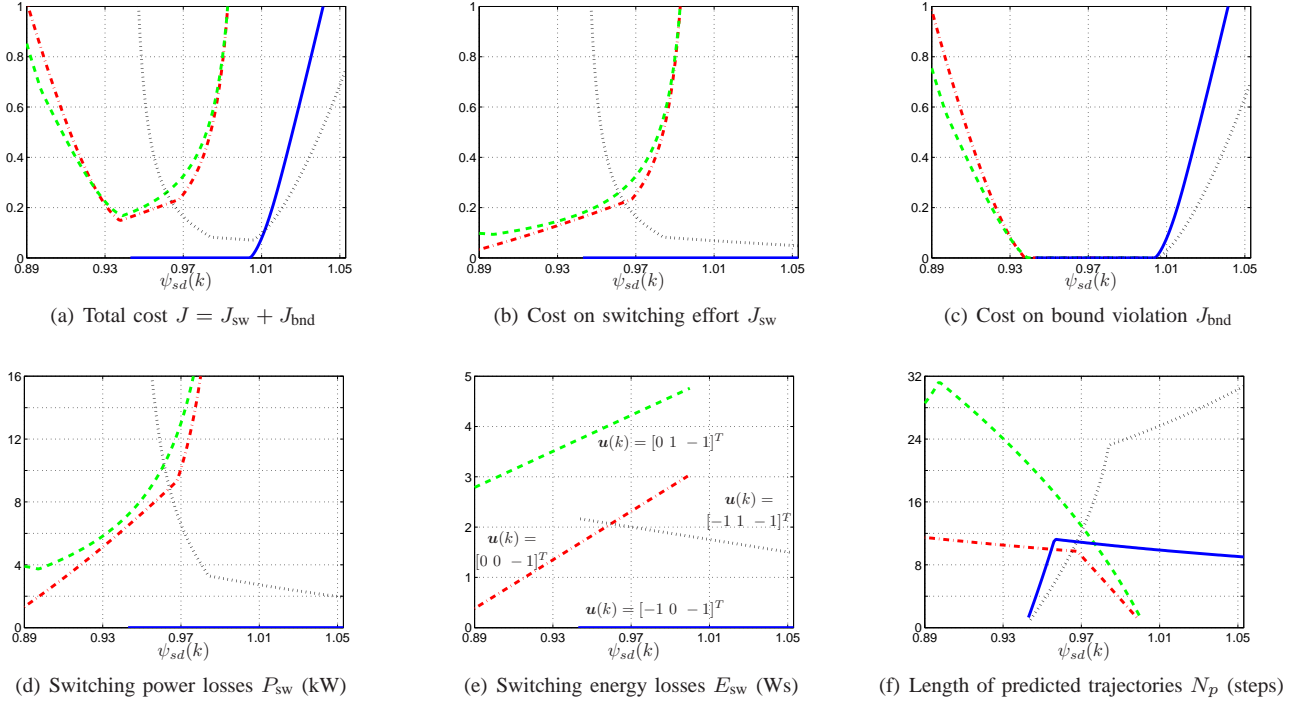


Fig. 6: Visualization of the control law derivation along the line  $\psi_{sd} \in [0.89, 1.054]$  pu and  $\psi_{sq} = 0.235$  pu. Four out of the 12 possible switch positions are considered: straight (blue) lines refer to keeping the current switch position, i.e.  $\mathbf{u}(k) = \mathbf{u}(k-1) = [-1 \ 0 \ -1]^T$ , dash-dotted (red) lines imply switching phase *a*, i.e.  $\mathbf{u}(k) = [0 \ 0 \ -1]^T$ , dotted (black) lines refer to switching phase *b*, i.e.  $\mathbf{u}(k) = [-1 \ 1 \ -1]^T$ , while dashed (green) lines relate to the case in which phases *a* and *b* are switched, i.e.  $\mathbf{u}(k) = [0 \ 1 \ -1]^T$

operating point to  $\omega_e = 0.1$ . The stator flux trajectories are now effectively straight lines and the zero voltage vector leads to a very slow stator flux movement.

So far, we have investigated control laws only for the case with the angle of the rotor flux vector being  $\varphi(k) = 0^\circ$ . Fig. 4(f) shows the control law for  $\varphi(k) = 30^\circ$ .

### E. Visualization of the Control Law Derivation

Additional insight in the derivation of the state-feedback control law is provided hereafter. For this, consider the control law along the line given by  $\psi_{sd} \in [0.89, 1.054]$  pu and  $\psi_{sq} = 0.235$  pu, which corresponds to the torque reference. This line is equivalent to a slice through the state-space  $\mathcal{X}$ . As previously, the current switch position is  $\mathbf{u}(k-1) = [-1 \ 0 \ -1]^T$ , from which transitions to 11 different switch positions are possible, in accordance with the constraint (5e). In Fig. 6 we consider only four options—keeping the current switch position and switching to three new ones. For some state vectors, certain options are not possible, e.g. for  $\psi_{sd} < 0.94$  keeping the current switch position would violate the constraint (5d).

Fig. 6(f) shows the lengths of the predicted stator flux trajectories. Due to the rotation of the reference frame, these lines are slightly curved, but they also exhibit distinctive changes in their slopes. The latter result when the bound, at which the trajectory terminates, changes. Below  $\psi_{sd} < 0.955$ , the straight (blue) line terminates at the lower flux bound, while above this threshold it terminates at the lower torque bound, see also Fig. 4(a).

The switching energy losses in Ws depend on the commutated stator current, which in turn is a linear combination of

the stator and rotor flux vectors. The switching energy losses thus depend linearly on the stator flux components. This is confirmed by the characteristically straight lines in Fig. 6(e). The different slopes result from the fact that the three stator current components sum up to zero.

The cost on the switching effort in Fig. 6(b) is obtained by dividing the switching energy losses by the trajectory lengths, as explained earlier. Therefore, these costs are—similar to the trajectory lengths—slightly curved lines with discontinuities. The switching power losses in Fig. 6(d) result by scaling Fig. 6(b).

The cost on violating a bound is zero, as the stator flux trajectory remains with the target window. This is the case when its initial state is within the window, as shown in Fig. 6(c). As the starting point of the stator flux trajectory moves away from the target window, the cost on the bound violation increases in an approximately quadratic fashion, due to the quadratic formulation used in (9). The slopes differ between the various switch positions, according to the predicted rms violation of the bounds. For  $\psi_{sd} > 1$ , for example, the switch position  $\mathbf{u}(k-1) = [-1 \ 1 \ -1]^T$  brings the stator flux vector significantly faster back into the target window than  $\mathbf{u}(k-1) = [-1 \ 0 \ -1]^T$  does. This is obvious from Fig. 4(a) and is reflected in Fig. 6(c).

The total cost  $J$  in Fig. 6(a) is the sum of the costs on the switching effort and on the bound violation, which are shown in Figs. 6(b) and 6(c), respectively. Based on this cost the optimal control input  $\mathbf{u}^*(k)$  is chosen. For  $\psi_{sd} < 0.94$ ,  $\mathbf{u}(k-1) = [0 \ 0 \ -1]^T$  and  $\mathbf{u}(k-1) = [0 \ 1 \ -1]^T$  yield similar costs. The first switch position incurs a lower switching effort, but tends to be slower in bringing the stator flux vector back

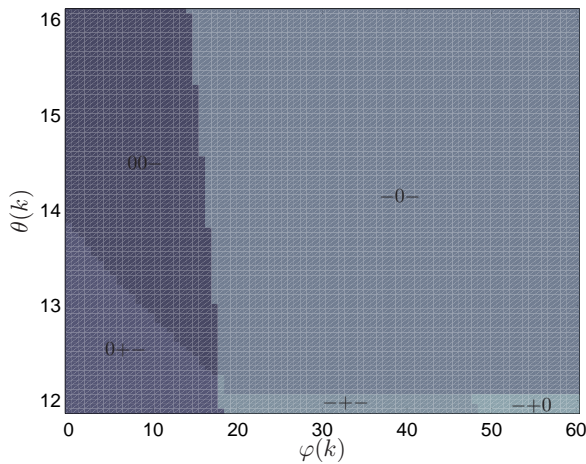


Fig. 7: State-feedback control law along the lower flux bound of the target window for  $\mathbf{u}(k-1) = [-1 \ 0 \ -1]^T$ , where  $\varphi$  represents the angular position of the rotor flux vector and  $\theta$  the (load) angle between the stator and rotor flux vectors

into the target window. Therefore, in the interval  $0.92 < \psi_{sd} < 0.94$ , the former is chosen as the optimal control input  $\mathbf{u}^*(k)$ , while for  $\psi_{sd} < 0.92$  the latter is optimal. Within the target window and when slightly violating the upper flux bound, i.e. for  $0.94 < \psi_{sd} < 1.00$ , it is optimal to not switch, i.e. to use  $\mathbf{u}^*(k) = \mathbf{u}(k-1)$ . For significant violations of the upper flux bound, i.e. for  $\psi_{sd} > 1.00$ ,  $\mathbf{u}^*(k) = [-1 \ 1 \ -1]^T$  is optimal.

## VI. CONTROL LAW ALONG AN EDGE OF THE TARGET WINDOW

During steady-state operating conditions, when the stator flux vector is kept within the target window, we have seen in the previous section that switching is performed effectively only along the edges of the target window. To gain insight into the dependency of the control law for varying the rotor flux angles, one can compute the control law for different  $\varphi$ , as exemplified in Fig. 4(f). Alternatively, one can compute the control law over a two-dimensional space, spanned by the rotor angle and the position along one of the edges of the target window. This is done separately for each edge. The lower flux bound, for example, can be parameterized in polar coordinates using the amplitude  $\Psi_s = \psi_{s,\min}$  and the load angle  $\theta$ , which was defined as the angle between the two flux vectors.

The result is shown in Fig. 7, with the angles given in degrees. As expected, the control law for  $\varphi = 0^\circ$  in Fig. 7 is identical to the one in Fig. 4(a) along the left edge of the target window (lower flux bound). The same holds for  $\varphi = 30^\circ$  and Fig. 4(f). Due to symmetry properties, it suffices to compute the control law over an angle span of  $60^\circ$  for  $\varphi$  to fully characterize the controller. The switching effort can be also plotted, similar to Fig. 5.

## VII. CONCLUSIONS

In model predictive control, including MPDTC, the control law is not directly available, unlike in FOC or DTC. This paper showed a straightforward method to compute the state-feedback control law. The derivation and visualization of the control law is paramount during the design process of the controller, since it enables one to analyze the controller's choices, to assess the impact of different objective functions, to understand the impact of switching constraints, and to evaluate

the influence of phenomena such as model uncertainties, observer noise and unaccounted for dc-link voltage fluctuations. Along with plotting the predicted trajectories, the availability of this method constitutes one of the main advantages of MPC over classic control methods, for which the design and tuning process is usually restricted to running closed-loop simulations.

Furthermore, with this tool at ones disposal, the following tasks are envisioned to be achieved in the near future: stability analysis, feasibility analysis, reduction of the computational effort, derivation of switching heuristics and a further improvement of the closed-loop performance. Moreover, this tool can be used equally well for other predictive drive control concepts, such as [12] and [17]. It is also straightforward to address multi-level inverter topologies and to include the neutral point potential in the considerations.

## ACKNOWLEDGMENT

A research grant from ABB Corporate Research, Baden-Dättwil, Switzerland is gratefully acknowledged by the author.

## REFERENCES

- [1] T. Geyer. *Low Complexity Model Predictive Control in Power Electronics and Power Systems*. PhD thesis, Autom. Control Lab. ETH Zurich, 2005.
- [2] T. Geyer, G. Papafotiou, and M. Morari. Model predictive direct torque control—Part I: Concept, algorithm and analysis. *IEEE Trans. Ind. Electron.*, 56(6):1894–1905, Jun. 2009.
- [3] T. Geyer. Generalized model predictive direct torque control: Long prediction horizons and minimization of switching losses. In *Proc. IEEE Conf. Decis. Control*, pages 6799–6804, Shanghai, China, Dec. 2009.
- [4] C. E. García, D. M. Prett, and M. Morari. Model predictive control: Theory and practice—A survey. *Automatica*, 25(3):335–348, Mar. 1989.
- [5] J. B. Rawlings and D. Q. Mayne. *Model predictive control: Theory and design*. Nob Hill Publ., Madison, WI, USA, 2009.
- [6] K. H. J. Chong and R.-D. Klug. High power medium voltage drives. In *Proc. IEEE Int. Conf. Power Syst. Technol.*, pages 658–664, Singapore, Nov. 2004.
- [7] I. Takahashi and T. Noguchi. A new quick response and high efficiency control strategy for the induction motor. *IEEE Trans. Ind. Appl.*, 22(2):820–827, Sep./Oct. 1986.
- [8] F. Blaschke. A new method for the structural decoupling of ac induction machines. In *IFAC Symp.*, pages 1–15, Oct. 1971.
- [9] T. Geyer. A comparison of control and modulation schemes for medium-voltage drives: emerging predictive control concepts versus field oriented control. In *Proc. IEEE Energy Convers. Congr. Expo.*, pages 2836–2843, Atlanta, GA, USA, Sep. 2010.
- [10] T. Geyer and G. Papafotiou. Model predictive direct torque control of a variable speed drive with a five-level inverter. In *Proc. IEEE Ind. Electron.*, pages 1203–1208, Porto, Portugal, Nov. 2009.
- [11] T. Geyer and S. Mastellone. Model predictive direct torque control of a five-level ANPC converter drive system. In *Proc. IEEE Energy Convers. Congr. Expo.*, Phoenix, AZ, USA, Sep. 2011.
- [12] R. Vargas, P. Cortés, U. Ammann, J. Rodríguez, and J. Pontt. Predictive control of a three-phase neutral-point-clamped inverter. *IEEE Trans. Ind. Electron.*, 54(5):2697–2705, Oct. 2007.
- [13] S. Mastellone, G. Papafotiou, and E. Liakos. Model predictive direct torque control for MV drives with LC filters. In *Proc. Eur. Power Electron. Conf.*, pages 1–10, Barcelona, Spain, Sep. 2009.
- [14] P. C. Krause, O. Wasynczuk, and S. D. Sudhoff. *Analysis of Electric Machinery and Drive Systems*. Intersci. Publ. John Wiley & Sons Inc., 2nd edition, 2002.
- [15] Y. Zeinaly, T. Geyer, and B. Egardt. Trajectory extension methods for model predictive direct torque control. In *Proc. App. Power Electron. Conf. and Expo.*, pages 1667–1674, Fort Worth, TX, USA, Mar. 2011.
- [16] T. Geyer. Computationally efficient model predictive direct torque control. In *Proc. IEEE Energy Convers. Congr. Expo.*, pages 207–214, Atlanta, GA, USA, Sep. 2010.
- [17] T. Geyer. Model predictive direct current control for multi-level inverters. In *Proc. IEEE Energy Convers. Congr. Expo.*, pages 4305–4312, Atlanta, GA, USA, Sep. 2010.